Marangoni convection in binary mixtures

Jie Zhang* and Robert P. Behringer†
Department of Physics and Center for Nonlinear and Complex Systems, Duke University, North Carolina 27708, USA

Alexander Oron‡
Department of Mechanical Engineering, Technion-Israel Institute of Technology, Haifa 32000, Israel
(Received 27 November 2006; revised manuscript received 14 May 2007; published 16 July 2007)

Marangoni instabilities in binary mixtures in the presence of the Soret effect and evaporation are different from those in pure liquids. In contrast to a large amount of experimental work on Marangoni convection in pure liquids, such experiments in binary mixtures are not available in the literature, to our knowledge. Using binary mixtures of NaCl/water in an open system, evaporation of water molecules at the liquid-vapor interface is inevitable. We have systematically investigated the pattern formation for a set of substrate temperatures and solute concentrations in an open system. The flow patterns evolve with time, driven by surface-tension fluctuations due to evaporation and the Soret effect, while the air-liquid interface does not deform. A shadow-graph method is used to follow the pattern formation in time. The patterns are mainly composed of polygons and rolls. The mean pattern size first decreases slightly, and then gradually increases during the evolution. Evaporation affects the pattern formation mainly at the early stages and the local evaporation rate tends to become spatially uniform at the film surface. The Soret effect becomes important at the later stages and affects the mixture for a large mean solute concentration where the Soret number is significantly above zero. The strength of convection increases with the initial solute concentration and the substrate temperature. Our findings differ from the theoretical predictions in which evaporation is neglected.

DOI: 10.1103/PhysRevE.76.016306 PACS number(s): 47.20.Dr, 47.15.gm, 47.54.−r, 68.15.+e

I. INTRODUCTION

When a horizontal pure-liquid thin film is sandwiched between a warm solid at the bottom and a cool gas at the top, heat transfer can be used to drive fluid flows. At the liquid-gas interface, the surface tension is a function of the interfacial temperature, and usually decreases with temperature. A small temperature perturbation along the film surface may create surface-tension inhomogeneities which in turn trigger fluid instabilities. Flows observed in such films are known as Bénard-Marangoni convection or surface-tension-driven convection. Several recent theoretical and experimental studies are relevant here [1–4]. Differing from thin films of pure liquids, the instabilities in binary-mixture films occur because the surface tension is a function of both temperature and solute concentration [5–9]. Given a vertical temperature gradient across the film, the concentration gradient may then be imposed by an independent source generated spontaneously by the Soret effect [10] or produced by evaporation of the solvent or solute at the liquid-gas interface. When a concentration gradient is caused solely by the Soret effect, theoretical work in the past decade has showed that if the thermal and solutal Marangoni effects enhance each other, a long-wavelength monotonic instability is possible. However, if they compete with each other, an oscillatory instability may occur instead. In both cases various linear and nonlinear theories of instability in thin films of binary mixtures with an ambient gas layer at the top have been developed [5–9]. By contrast, experiments with surface-tension-driven instabilities in binary mixtures are not available in the literature, to our knowledge. The lack of such experiments has motivated us to investigate pattern formation for binary mixtures in thin films. However, as discussed below, most commonly accessible binary mixtures are subject to evaporation of the solute, solvent, or both. Therefore, in our present system, both the Soret effect and evaporation are present, which is novel with no exact match to existing theory [5–9].

II. GOVERNING EQUATIONS AND PARAMETERS OF THE SYSTEM

The governing equations of the system, including the Soret effect are [7,9]

$$\vec{\nabla} \cdot \vec{v} = 0, \tag{1}$$

$$\partial_t \vec{v} + (\vec{v} \cdot \vec{\nabla})\vec{v} = -\rho^{-1}\vec{\nabla} p + \nu \nabla^2 \vec{v} - \vec{g}, \tag{2}$$

$$\partial_t T + (\vec{v} \cdot \vec{\nabla})T = \kappa \nabla^2 T, \tag{3}$$

$$\partial_t c + (\vec{v} \cdot \vec{\nabla})c = D(\nabla^2 c + s\nabla^2 T). \tag{4}$$

Here t is time, $\vec{v}$, p, ρ, ν, and $\vec{g}$ denote the fluid velocity field, pressure, density, kinematic viscosity, and gravitational acceleration, respectively, T and κ represent the temperature and thermal diffusivity of the fluid, respectively, c is the concentration of the solute, D is mass diffusivity of the solute, and s is the Soret coefficient.

In Eq. (3), the heat flux induced by the concentration gradient, known as the Dufour effect, is usually very weak in

*jz26@phy.duke.edu
†bob@phy.duke.edu
‡meroron@tx.technion.ac.il

liquids, and thus neglected due to the fact that the inverse Lewis number for liquids is large [11–14]. At the solid-liquid interface, $z=0$, $\vec{v}$ satisfies the no-slip, no-penetration condition $\vec{v}=0$, the temperature is fixed $T=T_w$, and the mass flux vanishes $c_z+sT_z=0$. Here, the substrate temperature T_w, i.e., the temperature at the bottom of the layer, is constant. At a nondeformable liquid-air interface $z=h(t)$, the boundary conditions are given by Ref. [15]. The heat and mass flux balances as well as those for the normal and tangential stresses read, respectively,

$$k_T T_z + q(T - T_a) + j\mathcal{L} = 0, \tag{5}$$

$$-\rho D(c_z + sT_z) + jc = 0, \tag{6}$$

$$j = \rho(w - h_t) = \hat{K}(T - T_a), \tag{7}$$

$$-\frac{j^2}{\rho_v} = -p + 2\mu w_z, \tag{8}$$

$$\mu(\partial_z \vec{u} + \nabla w) = -\sigma_T \vec{\nabla} T + \sigma_c \vec{\nabla} c. \tag{9}$$

Here, k_T is the thermal conductivity of the liquid, $\vec{u}$ is the two-dimensional projection of $\vec{v}$ onto the x-y (horizontal) plane, q is the heat transfer coefficient, assuming Newton's law of cooling, T_a is the constant room temperature, j is the evaporative mass flux, μ is the liquid viscosity, ρ_v is the vapor density, and $\mathcal{L}$ is the latent heat of evaporation. Also, we have assumed that the surface tension σ is a linear function of T and c; hence, $\sigma(T,c)=\sigma_0-\sigma_T(T-T_0)+\sigma_c(c-c_0)$. Here, σ_0 is the reference surface tension at $T=T_0$ and $c=c_0$. $\sigma_T \equiv -\left(\frac{\partial\sigma}{\partial T}\right)_{T_0}$ and $\sigma_c \equiv \left(\frac{\partial\sigma}{\partial c}\right)_{c_c}$. ΔT is the temperature difference across the film.

The dimensionless parameters of the problem are

$$P = \frac{\nu}{\kappa}, \quad L^{-1} = \frac{\kappa}{D}, \quad B = \frac{qh}{k_T}, \quad M = \frac{\sigma_T \Delta T h}{\rho \nu \kappa}, \tag{10}$$

$$E = \frac{k_T \Delta T}{\rho \nu \mathcal{L}}, \quad K = \frac{k_T \hat{K}}{h\mathcal{L}}, \quad \chi = \frac{s c_0 \sigma_c}{\sigma_T}, \quad \mathrm{Ra} = \frac{\alpha g \Delta T h^3}{\nu \kappa}, \tag{11}$$

respectively, the Prandtl, inverse Lewis, Biot, Marangoni, evaporation, interfacial resistance, Soret number, and Rayleigh number. The Soret number, which is defined here as the ratio of the concentration-induced surface-tension gradient (Soret effect) to the temperature-induced surface-tension gradient, is different from the separation ratio defined in buoyancy-driven binary convection [16]. However, they are related through appropriate derivatives of the density and surface tension. Table I shows a list of parameters for the concentrations relevant to our experiments. The estimate of the Soret number is based on the experimental data from Ref. [17]. Using the values in the table for a film of thickness $h=2$ mm, solute concentration of 2 M/l (Mole per liter of water), at the temperature 30 °C and $\Delta T=1$ °C, the estimated values of these dimensionless parameters are $P=6.06$, $L^{-1}=88$, $\chi=0.03$, $E=2.5\times10^{-4}$, $K=2.5\times10^{-5}$, $B=6$

TABLE I. The kinematic viscosity ν, thermal diffusivity κ, mass diffusivity of NaCl D, the density ρ, thermal conductivity k_T, concentration gradient of surface tension σ_c, temperature gradient of surface tension σ_T, the Soret coefficient s, and thermal expansion coefficient α as functions of different concentrations of NaCl at 30 °C. Majority values are obtained from CRC handbook of chemistry and physics unless otherwise stated.

NaCl concentration (Mol L^{-1})	0	0.06	0.8	2	4
$\nu(10^{-2}$ cm^2 s$^{-1})$	0.8	0.805[a]	0.836[a]	0.904[a]	1.096[a]
$\kappa(10^{-3}$ cm^2 s$^{-1})$	1.479	NA	1.467[c]	1.491[c]	1.514[c]
$D(10^{-5}$ cm^2 s$^{-1})$	NA	1.72[a]	1.71[a]	1.70	1.64[a]
ρ(g cm^{-3})	0.995	0.998[a]	1.027[a]	1.070	1.134
$k_T(10^4$ erg cm^{-1} s^{-1} K$^{-1})$	6.154	6.071[a]	6.081[a]	6.005[a]	5.897[a]
σ_c(dyne cm^{-1} mol^{-1} L)	1.5[b]	1.5[b]	1.5[b]	1.5[b]	1.5[b]
$\sigma_T(10^{-2}$ dyne cm^{-1} K$^{-1})$	16.1	16.1[b]	16.1[b]	16.1[b]	16.1[b]
$\mathcal{L}(10^{10}$ erg/g)	2.43[d]	2.43	2.43	2.43	2.43
$s(10^{-3}$ K$^{-1})$	NA	−1.5	0.92	1.5	2
$\alpha(10^{-4}$ K$^{-1})$	3.03	3.07[a]	3.49[a]	3.95	4.33

[a]Linear interpolation.
[b]Data are obtained from Ref. [18] which shows that σ_T and σ_c are independent of temperature and concentration.
[c]These numbers are interpolated from Ref. [26].
[d]In the CRC book, the latent heat is referred to as enthalpies-of-vaporization, which is essentially the same for a NaCl solution as well as for pure water.

$\times10^{-3}$, Ra=230, and $M=2232$. This value of the Marangoni number is significantly higher than the standard value of $\approx$80 for the threshold of surface-tension-driven convection [1,3,4]. This is related to the fact that evaporation of a water particle can significantly cool down the surface temperature and create a large temperature drop across the film. The Prandtl and inverse Lewis numbers show the relative diffusion speeds of momentum versus heat transfer and heat versus mass transfer. The product of the Soret number and the inverse Lewis number represents the contribution of the solutal effect to the surface-tension fluctuations with respect to that of the thermal effect. A small Biot number suggests that the gas layer at the top is a poor heat conducting phase compared to the liquid. The Rayleigh and Marangoni numbers characterize the relative strength of the driving by buoyancy and surface tension, respectively, with respect to the dissipation provided by thermal diffusivity and kinematic viscosity of the fluid. A small value of the evaporation number E corresponds to slow evaporation rate, while small values of the value K correspond to a low interfacial resistance to phase change. As long as the film thickness is below 2 mm, which is typical in our experiment, the Rayleigh number is well below the threshold value 1101 and thus, the buoyancy effect is not important in our system. In the case of a film thickness of 2 mm and the material properties given in Table I, the time scales of mass, heat and momentum diffusion can be estimated as $\frac{h^2}{D}=40$ min, $\frac{h^2}{\kappa}=27$ s, and $\frac{h^2}{\nu}=4.4$ s. It thus follows that in order for the solutal effects to play a role, a sufficiently long time of at least 40 min has to elapse.

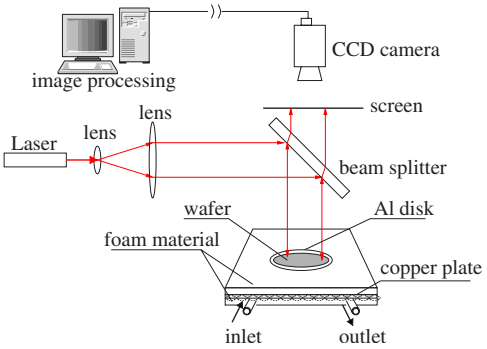

FIG. 1. (Color online) Schematic of the experimental setup. Visualization is by standard shadowgraph using an expanded laser beam for a light source. The bottom plate of the cell that contains the film consists of a highly reflecting silicon wafer that is thermally grounded to a highly conducting copper plate. This plate is temperature controlled by means of a regulated water bath.

III. EXPERIMENTAL SYSTEM

Before carrying out an experiment, the first important issue to be resolved is the selection of a reasonably nonvolatile working liquid, i.e., a binary liquid. We explored a wide range of candidate materials. We first tried a mixture of ethanol and water and then abandoned it due to the fast evaporation of ethanol. We also tested different combinations of silicone oils with noticeable differences in surface tension between them to avoid nonmiscibility. Only a few silicone oils satisfying the requirements of nonvolatility and miscibility are commercially available and affordable. However, for all the possible pairs of oils, either one or both are highly volatile at room temperature or they are highly viscous at low temperature and volatile when heated. The volatilities are typically much larger than that of pure water. As a consequence, we did not choose binary mixtures of silicone oils for our experiments. Finally, we chose solutions of sodium chloride (NaCl) with pure water as the working binary mixtures. There is an additional advantage in choosing the mixture of NaCl/water as a working liquid because its many physicochemical properties are available in the literature, including surface tension as a function of both concentration and temperature [18], and the variation of the Soret coefficient with temperature and concentration [17] among others. The evaporation of water is significantly weaker than that of other strongly volatile liquids, so that there is a reasonably long time to take measurements before the film dries out completely. Finally, the convective patterns are readily visible a short time after a thin film is drawn.

Figure 1 presents a sketch of the experimental setup of the system. The film was prepared on top of a silicon wafer with a circular Plexiglas ring (about 7 cm in diameter) as the lateral boundary. The wafer was bonded to an Aluminum disk attached to a thin copper plate. A copper tubing coil was soldered to the bottom of the latter. The two ends of the coil were connected to a water bath (Neslab RTE-221) using thermally insulated plastic tubing. The temperature of the plate was held constant by water circulation. To further reduce the heat loss, the whole copper plate was covered by thermally insulating foam materials, leaving only a circular hole to hold the Aluminum disk. The film was directly exposed to the room air whose temperature is approximately constant during the course of an experiment.

Temperature variations at the liquid surface may come from four different sources: transport and mixing of the convective fluid, evaporative latent heat loss, the fact that the wafer is not an ideal uniform-temperature source, and temperature fluctuations of the air layer at the top. The first two are of the order of the temperature difference ΔT across the liquid and are intrinsic to the fluid convection itself. The last two sources are unwanted and can be experimentally minimized. The temperature in the room air is controlled by the room thermostats and is monitored with a thermometer. The temperature fluctuation in the room air is $\pm 0.5\ ^\circ\mathrm{C}$. Such a fluctuation is roughly equivalent to a fluctuation by $\sim(0.5 \times B)\ ^\circ\mathrm{C} \approx 3$ mK of the base temperature. Here, B is the Biot number, see Eq. (10), $\sim 6 \times 10^{-3}$. In the above estimate, we assume that there is no thermal convection in the air layer. Of course, the air layer could, in reality, be convective. To verify that air convection is not an issue, and therefore test the validity of this estimate, we measured the temperature fluctuation at the surface of a 2 mm thick pure water film with room temperature at 20 °C and substrate temperature around 30 °C. We did this by placing a thermistor just at the fluid interface. The temperature fluctuation at the surface is about 10 mK which is about three times larger than the estimate. In addition, no convective patterns were found, which indicates that there is no entrained fluid motion by a possibly convective air flow at the top.

The temperature fluctuation of the wafer was affected by several sources. The first source is the thermal fluctuation of the Neslab water bath which does not exceed 10 mK. The second source is the temperature fluctuation at the liquid-air interface. To further reduce the thermal fluctuation at the silicon wafer, a bridge-controlled heating method was applied [19]. The substrate temperature was measured by a thermistor embedded underneath the wafer which was measured with an ac bridge. An offset of the bridge balance point drove an integrodifferential feedback circuit which, in turn, drove a heater attached to the inlet of the tubing that carried the cooling water. In such a way, the thermal fluctuation of the wafer was further reduced. Depending on the mean temperature of the film, the long-time thermal fluctuations of the substrate temperature are less than 30 mK at the mean temperature of the film $T_f \equiv T_w - \frac{1}{2}\Delta T \approx 30\ ^\circ\mathrm{C}$ and less than 15 mK at $T_f \approx 25\ ^\circ\mathrm{C}$. The mean temperature drop across the film ΔT is typically less than 1 °C.

IV. RESULTS AND DISCUSSION

Figure 2 shows a set of typical shadowgraph flow patterns observed in thin films of NaCl-water mixtures with an initial NaCl concentration of 4 M/l. In particular, in this figure bright and dark shades correspond to downward and upward flows, respectively, as tested by depositing a few dust particles on the film surface. The optical signals of the shadow graph are due to the bending of the parallel light through the changes of the index of reflection in the film. The change of the index of reflection is due to both the temperature and

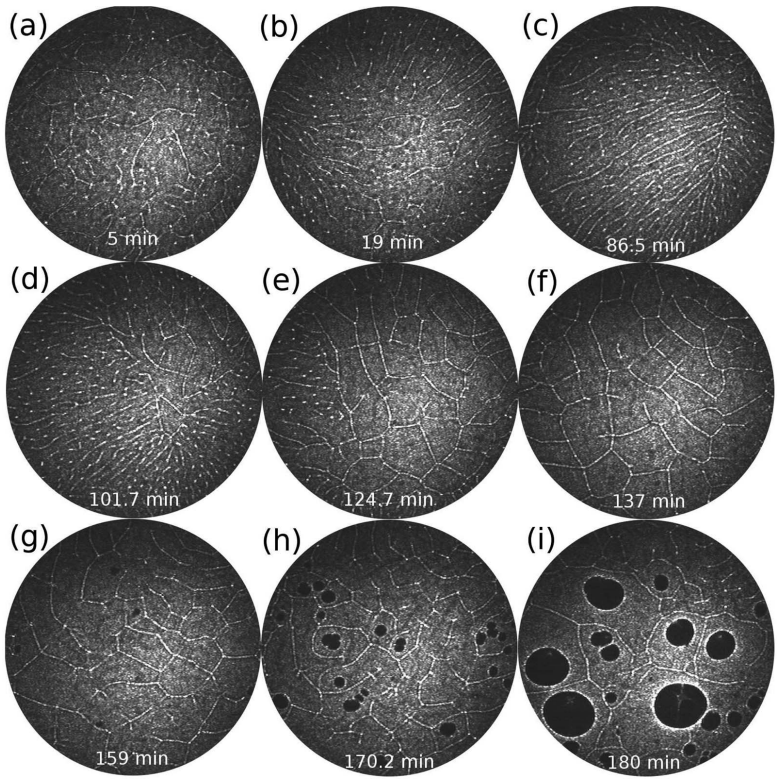

FIG. 2. Convection patterns observed at a film temperature $T_f=30\ ^\circ\mathrm{C}$ and a room temperature $T_a=20\ ^\circ\mathrm{C}$. The initial concentration of NaCl is $c_0=4$ M/l and the initial film thickness is $h_0=1.8$ mm. Images (a)–(i) show the flow pattern at nine different times t. Bright and dark shades, correspond to downward and upward flows, respectively. The black spots in images (h) and (i) represent the growing salt crystals. The estimated initial Marangoni number is $M_0=2122$. The size of each image corresponds to 3.55 cm in reality.

concentration fields. In general, the judgment about the flow directions are not as straightforward as in Marangoni convection in pure liquids (MCP). These patterns are very irregular and evolve with time. Following the film deposition, an irregular pattern emerges, as seen in Fig. 2(a). This is a transient process with patterns gradually decreasing in size [Fig. 2(b)]. Eventually small-scale patterns cover the entire system, as shown in Fig. 2(c). The majority of the patterns are rolllike structures, although there are also localized dots, which are rarely observed in MCP. These small-scale patterns persist for a period of time before any qualitative changes appear. Then, the characteristic scale of the pattern becomes larger and the patterns consist primarily of polygons, as shown in Figs. 2(d)–2(f). If the concentration of NaCl exceeds the maximal solubility ($\approx$8 M/l), salt begins to crystallize out of the solution; small islands of salt appear as black dots, as in Fig. 2(g)–2(i). An interesting aspect of the system evolution concerns the film thickness. Interferometric measurements show that except at the meniscus boundary, the film thickness remains horizontally uniform during the evolution preceding the formation of salt crystals when deformation of the film interface becomes significant.

To quantify the time variation of the pattern size, we apply fast Fourier transforms (FFT) to the original shadowgraph images after the removal of the background intensity variation. The images in the Fourier space were averaged over phase angles. The inset of Fig. 3 shows two typical azimuthally averaged spectra at two different times. The two spectra are clearly separated. From the FFT spectrum, we calculate both the mean wave number and its standard deviation. The results are then converted to a real space pattern size $s(t)$ as presented in Fig. 3(a) for $T_f=30\ ^\circ\mathrm{C}$. We normalize this characteristic pattern size by its instantaneous film thickness, which we refer to hereafter as the normalized pattern size. Immediately after the film is initialized, the normalized pattern size is approximately 0.8, i.e., the average pattern size is slightly below the value of the film thickness. For some time thereafter, the patterns are rolls, as seen in Fig. 2(c). The normalized pattern size also retains its initial value for a considerable time, and then gradually increases. Due to evaporation, the film thickness decreases monotonically. Because the Marangoni number is proportional to the film thickness, it too continuously decreases. Finally, the average normalized pattern size reaches $s/h\simeq 3.0$. At this point, the corresponding pattern consists mainly of nonequilateral polygons. The irregular shape of these polygons leads to large errors in determining the pattern size, Fig. 3. This feature is different from the classical MCP where patterns are regular polygons [1,20]. This difference may be caused by one or a combination of several sources. First, there is the fact that the surface conditions in the MCP are usually precisely controlled, as compared to the present open system, for which a precise control of the air layer above the film surface is much more difficult. Alternatively, we note that the estimated Marangoni number is much larger here than in MCP and is ever changing, as the system is never in a steady state, and it is impossible to tune the value of the Marangoni number exactly at the threshold value.

Towards the later stages of the pattern evolution, a noticeable difference in the pattern occurs as relatively linear rolls give way to polygonal patterns. At that point, the Marangoni number is 539 ± 29, which is quite big compared with the threshold values derived in nonevaporative films [5,6], and the film thickness was about 0.9 mm. A large Marangoni number was also observed in an experiment using pure liquid

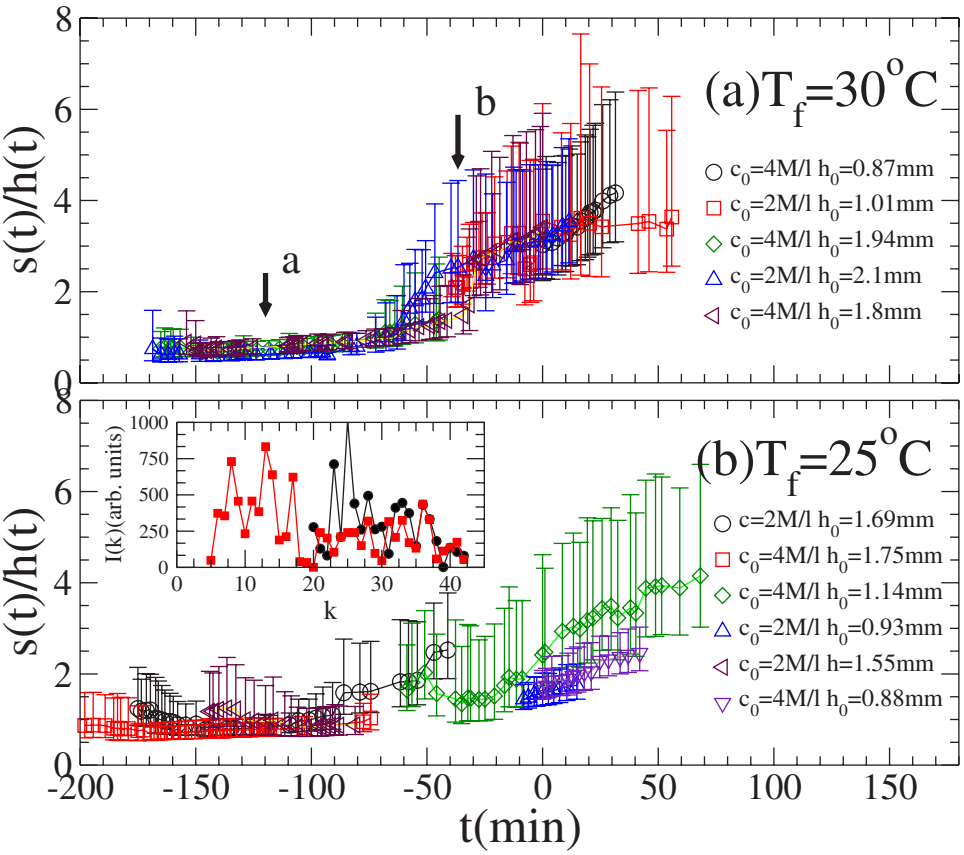

FIG. 3. (Color online) The average normalized pattern size $s(t)/h(t)$ as a function of time t. The time axis is chosen (thus negative times) so that different data sets have approximately the same film thickness $h(t)=0.9$ mm at $t=0$ min. Various symbols represent measurements performed at different initial concentrations c_0 of NaCl, different initial film thickness h_0, and different film temperatures T_f. The inset shows two typical azimuthally averaged spectra at two different times corresponding to the data marked by the triangles in (a), circles at arrow **a**, and squares at arrow **b**.

films with strong evaporation [21]. However, no patterns were observed in pure water films in our system. Marangoni convection in pure water is usually hard to detect, although it was indirectly observed in Ref. [22] with a different geometry and boundary condition, and directly observed in Refs. [23,24] with the complete suppression of evaporation. The absence of convection observed in pure water film suggests that thermocapillarity as a possible mechanism for instability of the quiescent state is not sufficiently strong in that case. Hence, the enhancement originating from the solutal effects, such as thermo-soluto-capillarity and Soret effect becomes important. This also leads us to the conjecture that the temperature at the surface of the water film may actually be horizontally uniform. Significant nonuniformities of the temperature there would imply the emergence of convection driven by the relatively large temperature drop across the film due to the latent heat loss. Note that Fig. 3 does not show data for times when the crystallization of NaCl (black dots) takes place at the film surface, as seen in Figs. 2(g)–2(i). The existence of the solid phase changes the flow pattern dramatically. For instance, solid NaCl can grow and merge with a deformable fluid interface. The physics of this stage has not yet been well understood and is outside the scope of this work.

Figure 3(b) shows the time evolution of the normalized pattern size at a different temperature $T_f=25$ °C. While the qualitative features are similar to Fig. 3(a) (where $T_f=30$ °C) there are still some quantitative differences. The normalized pattern size at the early stages is around 1.0 which is larger than 0.8 at $T_f=30$ °C. In the beginning of each run (see, e.g., circles and diamonds), the normalized pattern size usually decreases for the initial 10–20 min. This feature exists in some of the other runs in figures (a) or (b), except it is more visible here. We note that typically, after the film is deposited, patterns generally appear at a slightly bigger size; they then gradually decrease in size by developing smaller scale convection polygons or rolls such as those in Figs. 2(a)–2(c).

The normalized pattern-size variation for films with low concentrations have weaker convection flows and convection decays rapidly. For instance, in Fig. 4(a), for $c_0=0.4$ M/l, the patterns are readily seen at time $t=2.1$ min; they are very weak if not completely gone in (b) at $t=47.5$ min after the film is deposited. Similar observations were seen for initial concentrations $c_0 \leqslant 0.8$ M/l. The decay of the pattern is an indication that the local evaporation flux has a tendency to become spatially uniform with time. It is reasonable to believe that the evaporation rate, and hence this effect, should be independent of concentration. For higher concentrations, however, the patterns persist and the intensity tends to be more uniform during the evolution. One possibility is that this difference is related to the Soret coefficient, as deter-

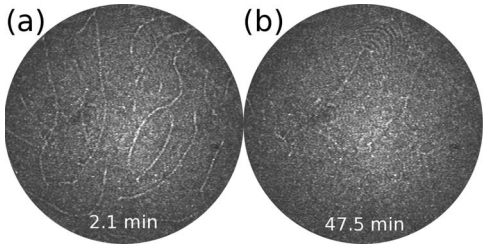

FIG. 4. Weakening of the convection intensity at $T_f \approx 30\ ^\circ\mathrm{C}$, $T_a = 22.2\ ^\circ\mathrm{C}$, initial concentration of NaCl $c_0 = 0.4$ M/l, and initial film thickness $h_0 = 2.2$ mm.

mined, for instance, from data for NaCl-water mixtures by Gaeta *et al.* [17] At $T = 30\ ^\circ\mathrm{C}$, the Soret coefficient is $\alpha \simeq 0$ at $c = 0.2$ M/l and linearly increases as $\log_{10} c$ to $\alpha = 1.5 \times 10^{-3}/^\circ\mathrm{C}$ at $c = 2$ M/l. We estimate the corresponding Soret number to be $\chi = 0.04$ for $c = 2$ M/l and $\chi = 0.10$ for $c = 4$ M/l. The characteristic time for mass diffusion, about 40 min for a 2 mm thick film, is roughly the same as in Fig. 4. This suggests that the Soret effect becomes important at the later stage of convection. In Fig. 4(b), the value $\chi \approx 0.002$ is too small to drive convection after the pattern created by evaporation begins fading away. Thus, in order for the Soret effect to play a role, a sufficiently large concentration leading to a higher Soret diffusion is necessary since the solutal Marangoni effect is directly proportional to the Soret number χ.

In our experiments we have measured the instantaneous thickness of the film over extended periods of time. Using the time history we then evaluate the evaporation rate as a function of time. We find that this quantity is nearly constant at a given film temperature T_f and a room temperature T_a. Considering that the mean concentration increases with time, the linear plot for $h(t)$, as seen in the Fig. 5(a), implies a very weak concentration dependence on the evaporation rate. The slope of $h(t)$ vs t increases for a larger film temperature T_f or a smaller room temperature T_a. The linear decrease of the film thickness due to evaporation seems to be robust and almost independent of the NaCl concentration. As a comparison, measurements of the film thickness for evaporating pure-water films are also presented in Fig. 5(a). The slope of $h(t)$ for a water film is also a constant, similar in size to what is obtained for the mixtures, indicating that this linear behavior is indeed independent of the composition of the liquid film.

This result is different from the analytical solution obtained by Burelbach *et al.* [25] and Oron *et al.* [15] for the base state of an evaporating film of a uniform thickness

$$h(t) = h_0[\sqrt{(K+1)^2 - 2Et} - K], \tag{12}$$

where h_0 is the initial film thickness, K is a constant interfacial resistance to phase change, and E is the evaporation constant. If $Et \ll 1$, $h(t)$ would be nearly linear. However, as Et grows, $h(t)$ would start to bend downwards, especially at small $h(t)$. This trend is not seen in the present data. We have experimentally ruled out the possibility that convective air motion above the film might be responsible, since the theory assumes that the air layer is at rest. In particular, experimental measurements of the evaporation rate for a film at a temperature lower than the room air are also presented in Fig. 5(a) shown by the triangle-left symbols; they too show a

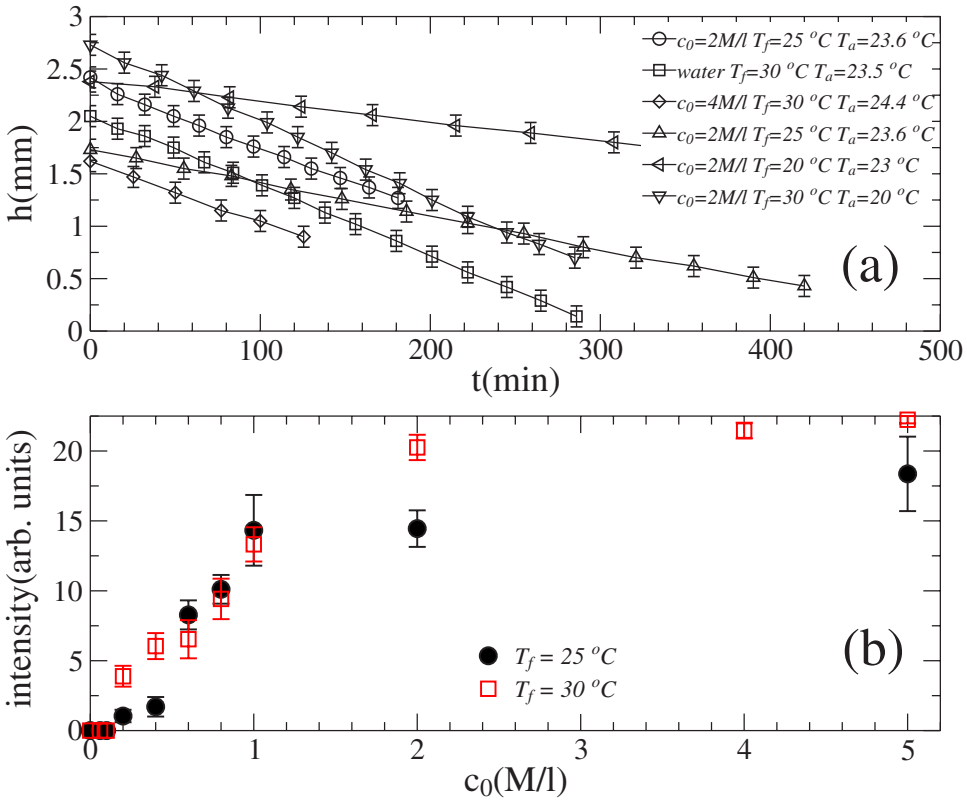

FIG. 5. (Color online) (a) The film thickness change as a function of time in the presence of evaporation. (b) The convection intensity as a function of the initial NaCl concentration c_0 and film temperature T_f with the room temperature $T_a = 20\ ^\circ\mathrm{C}$. No convection is observed for $c_0 < 0.2$ M/l.

linear variation. We suggest that the reason for the discrepancy between theory and experiment is due to the large change in the temperature gradient that occurs at the liquid-air interface, and that is associated with the extra heat transport needed to evaporate the liquid. Because the temperature gradient in the fluid remains nearly constant, the evaporation rate also remains constant. Hence, the boundary condition used in recent theoretical work differs from that which applies for these experiments.

Keeping other conditions the same, the magnitude of the convection, as determined based on the average intensity of the shadowgraph images recorded over the first 15 min after the film was initialized, depends on the initial concentration c_0 of NaCl and the film's mean temperature. At low concentrations $c_0 \leqslant 0.1$ M/l, there are no visible convection patterns even for a 2.2 mm thick film. This implies that buoyancy is irrelevant in our system if we assume that the thermal expansion of the fluid is not significantly affected by adding NaCl to the pure water. When the concentration c_0 is higher than 0.2 M/l, the patterns gradually appear. This observation suggests that thermal Marangoni effect alone cannot drive the fluid instability and that the fluid motion is driven by a combination of thermal Marangoni and solutal Marangoni effects. The magnitude increases monotonically with concentration for $c_0 \geqslant 0.2$ M/l. At a fixed film temperature of 30 °C, the Soret coefficient is negative in the concentration range 0.042 M/l $\leqslant c_0 \leqslant$ 0.13 M/l [17]. However, in such a range, the concentration is too low to observe any realistic motions in the film.

V. SUMMARY

To summarize, we have experimentally studied transient Marangoni convection in thin binary-mixture liquid films using solutions of NaCl and water in an open system. In the presence of evaporation, the patterns, consisting of rolls and polygons, evolve with time. The length scale of the pattern increases with time until the convection ceases. The Marangoni numbers near onset are much larger than the values predicted in theories developed for nonvolatile binary liquids. Evaporation is important to the pattern formation at the early stage, while the Soret effect is essential at the later stage. For higher concentrations of NaCl, the convection becomes stronger. Within the temperature range 25 °C $\leqslant T_f \leqslant$ 30 °C explored in the experiment, convection patterns were observed in the NaCl concentration range 0.2 M/l $\leqslant c_0 \leqslant$ 5 M/l. Understanding the rich pattern forming dynamics clearly requires new theoretical work.

ACKNOWLEDGMENTS

This work was supported by NSF Grant No. DMS-02444498. J.Z. thanks Matthias Sperl for his comments and suggestions of the manuscript. J.Z. also enjoyed the discussion with Peidong Yu about the lockin amplifier. A.O. acknowledges the hospitality of the focused research group in thin films and of the Mathematics department of Duke University. A. O. was partially supported by the Israel Science Foundation founded by the Israel Science Foundation through Grant No. 31/03-15.3.

[1] M. F. Schatz, S. J. VanHook, W. D. McCormick, J. B. Swift, and H. L. Swinney, Phys. Rev. Lett. **75**, 1938 (1995).
[2] S. J. VanHook, M. F. Schatz, W. D. McCormick, J. B. Swift, and H. L. Swinney, J. Fluid Mech. **345**, 45 (1997).
[3] S. H. Davis, Annu. Rev. Fluid Mech. **19**, 403 (1987).
[4] P. Colinet, J. C. Legros, and M. G. Velarde, *Nonlinear Dynamics of Surface-Tension-Driven Instabilities* (Wiley-VCH, Berlin, 2001).
[5] J. K. Bhattacharjee, Phys. Rev. E **50**, 1198 (1994).
[6] S. W. Joo, J. Fluid Mech. **293**, 127 (1995).
[7] A. Oron and A. A. Nepomnyashchy, Phys. Rev. E **69**, 016313 (2004).
[8] A. Podolny, A. Oron, and A. A. Nepomnyashchy, Phys. Fluids **17**, 104104 (2005).
[9] A. Podolny, A. Oron, and A. A. Nepomnyashchy, Phys. Fluids **18**, 054104 (2006).
[10] J. K. Platten and P. Costeseque, Eur. Phys. J. E **15**, 235 (2004).
[11] G. W. T. Lee, P. Lucas, and A. Tyler, J. Fluid Mech. **135**, 235 (1983).
[12] W. Hort, S. J. Linz, and M. Lücke, Phys. Rev. A **45**, 3737 (1992).
[13] J. Liu and G. Ahlers, Phys. Rev. E **55**, 6950 (1997).
[14] St. Hollinger, M. Lücke, and H. W. Muller, Phys. Rev. E **57**, 4250 (1998).
[15] A. Oron, S. H. Davis, and S. G. Bankoff, Rev. Mod. Phys. **69**, 931 (1997).
[16] A. La Porta and C. M. Surko, Phys. Rev. Lett. **80**, 3759 (1998).
[17] F. S. Gaeta, G. Perna, and F. Bellucci, J. Phys. Chem. **86**, 2967 (1982).
[18] M. Matubayasi, H. Matso, K. Yamamoto, S-i. Yamaguchi, and A. Matuzawa, J. Colloid Interface Sci. **209**, 398 (1999).
[19] R. P. Behringer and G. Ahlers, J. Fluid Mech. **125**, 219 (1982).
[20] H. Bénard, Rev. Gen. Sci. Pures Appl. **11**, 1261 (1900).
[21] A.-T. Chai and N.-L. Zhang, Exp. Heat Transfer **11**, 187 (1998).
[22] C. A. Ward and F. Duan, Phys. Rev. E **69**, 056308 (2004).
[23] A. Juel, J. M. Burgess, W. D. McCormick, J. B. Swift, and H. L. Swinney, Physica D **143**, 169 (2000).
[24] W. A. Tokaruk, T. C. A. Molteno, and S. W. Morris, Phys. Rev. Lett. **84**, 3590 (2000).
[25] J. P. Burelbach, S. G. Bankoff, and S. H. Davis, J. Fluid Mech. **195**, 463 (1988).
[26] J. Wang and M. Fiebig, Int. J. Thermophys. **19**, 15 (1998).